Composition effects on the early-stage oxidation kinetics of (001) Cu–Au alloys

G.-W. Zhou, J. A. Eastman,[a] R. C. Birtcher, P. M. Baldo, J. E. Pearson, and L. J. Thompson
Materials Science Division, Argonne National Laboratory, Argonne, Illinois 60439

L. Wang and J. C. Yang
Materials Science and Engineering Department, University of Pittsburgh, Pittsburgh, Pennsylvania 15261

(Received 28 August 2006; accepted 28 November 2006; published online 9 February 2007)

An *in situ* environmental transmission electron microscopy study of the nucleation and growth of oxide islands during the early-stage oxidation of (001) $Cu_{1-x}Au_x$ alloys ($x \leqslant 38$ at. %) was undertaken in order to investigate the effects of alloying on oxide island nucleation behavior and growth kinetics. The kinetic data reveal that Au enhances the nucleation density of oxide islands and suppresses their growth rate. Our results provide insight into reasons for the decreased passivation properties of Cu when alloyed with Au. © *2007 American Institute of Physics*.
[DOI: 10.1063/1.2433714]

I. INTRODUCTION

Alloying commonly leads to materials whose properties are substantially changed with respect to pure metals. One common application of alloying is in the development of materials with enhanced oxidation resistance, which results from the formation of a continuous oxide layer covering the metal surface. After fast early-stage oxidation limited only by the supply of oxygen to the surface, further reaction is then controlled by much slower diffusion of metal and/or oxygen through this continuous layer. Much progress has been made in understanding later-stage oxidation, as formulated by Wagner[1] and modified Wagner-type theories that account for short-circuit diffusion paths within the oxide layer.[2–4] The passivation behavior of metals is strongly influenced by the microstructures of the oxides that form. For example, a high density of short-circuit diffusion paths within the oxide layer often leads to poor oxidation resistance. The morphology of the oxide film can be strongly influenced by the oxide nucleation and early-stage growth behavior. However, detailed information from early-stage oxidation studies is still very limited, especially in the case of alloys. This is due primarily to the lack of tools capable of probing atomic level and mesoscale behavior *in situ* during the early stages of oxidation.

In situ ultrahigh vacuum (UHV) transmission electron microscopy (TEM) is an ideal tool to investigate early stages of metal oxidation. The advantages of *in situ* UHV TEM experiments include visualization of oxidation processes in real time and information on buried interfaces. Furthermore, this technique is capable of providing dynamic information from nucleation to initial growth and coalescence of oxide islands at nanometer scale under controlled surface conditions, which is inaccessible to both surface science methods and traditional bulk oxidation studies, but is essential for a fundamental understanding of atomistic oxidation kinetics. The early-stage oxidation of pure copper has been extensively investigated using *in situ* UHV TEM to gain insights into the atomistic mechanisms of metal oxidation. These studies have revealed that oxidation typically involves nucleation, growth, and coalescence of oxide islands and that oxide island growth is limited by surface diffusion of oxygen.[5–8] These observations represent a departure from classical theories which assume uniform, layer-by-layer growth of a coalesced film beginning with the first monolayer.[1,9]

Alloy oxidation is generally much more complex compared to the oxidation of pure metals. The possible effects of alloying elements on the oxidation behavior include different oxygen affinities of the alloying elements, formation of multiple oxide phases and solid solubility between them, various mobilities of metal ions in the oxide phase, and different diffusivities of metals in the alloy. Due to these complexities, alloy oxidation is still not well understood, especially the early stages of alloy oxidation. Choosing Cu–Au as a model system, we perform an *in situ* TEM study of the early-stage oxidation kinetics of alloys containing a noble metal and an oxidizable metal, and we seek the effects of alloying on nucleation, growth, and morphology of oxide islands. This system is considered since it allows some of the features of alloy oxidation to be examined without the complication of the simultaneous formation of two oxides. Also, at temperatures >410 °C, where oxidation behavior is of most interest, Cu and Au are fully miscible.

II. EXPERIMENTAL DETAILS

Our *in situ* oxidation experiments were carried out in a modified JEOL 200CX TEM.[10] This microscope is equipped with a UHV chamber with a base pressure $\sim 10^{-8}$ Torr. The microscope was operated at 100 keV to minimize the possibility of irradiation induced effects. A controlled leak valve attached to the column of the microscope permits introduction of gases directly into the microscope. Single crystal ~ 1000 Å (001)Cu–Au alloy thin films with different Au

[a]Author to whom correspondence should be addressed; electronic mail: jeastman@anl.gov

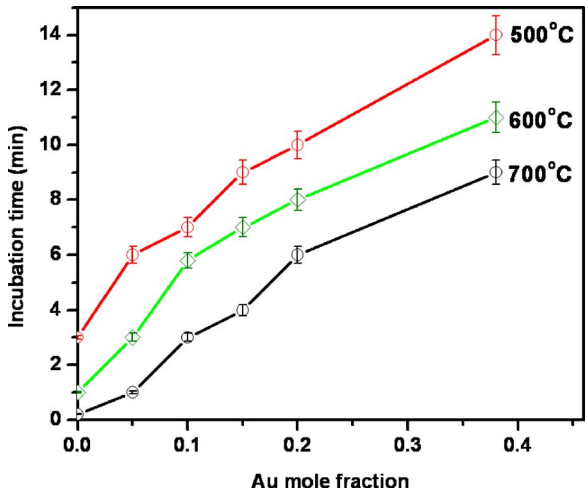

FIG. 1. (Color online) Composition and temperature dependence of the incubation time during oxidation of the Cu–Au alloys.

mole fraction were grown on irradiated (100)NaCl by sputter deposition. The film composition and thickness were calibrated by Rutherford backscattering (RBS). The alloy films were removed from the NaCl substrate by flotation in deionized water, washed and mounted on a specially designed TEM sample holder, which allows for resistive heating at temperatures between room temperature and 1000 °C. The native Cu oxide is removed by annealing the alloy films in the TEM under vacuum conditions at ~750 °C (Ref. 11) or by *in situ* annealing in methanol vapor at a pressure of 5×10^{-5} Torr but at a lower temperature (~350 °C),[12] resulting in a clean metal surface. Oxygen gas of 99.999% purity can be admitted into the column of the microscope through the leak valve at a partial pressure (pO_2) between 5×10^{-5} and 760 Torr. Real time observations can be made at pressures $\leqslant 8\times10^{-4}$ Torr.

III. RESULTS

A. Effect of composition on the nucleation of oxide islands

Our *in situ* TEM observations indicate that an incubation time is needed before the appearance of visible oxide nuclei on the metal surface after admitting oxygen into the microscope. The incubation time depends on oxidation temperature and alloy composition (Fig. 1). A longer incubation time is needed to nucleate oxide islands for the alloys with larger Au mole fractions. Increasing oxidation temperature leads to a decrease in the incubation time.

After the incubation period, oxide nuclei become visible, and their number increases with time and then saturates. The nucleation rate (from the appearance of the first nuclei to saturation density) also depends on the Au mole fraction in the alloy, and alloys with higher Au mole fractions exhibit faster nucleation rates. Figure 2(a) shows some examples of the oxide islands formed during Cu–Au oxidation at 600 °C in $pO_2=5\times10^{-4}$ Torr. Figure 2(b) shows the saturation density of oxide islands formed during the oxidation of (100)Cu–38 at. % Au at different temperatures in $pO_2=5\times10^{-4}$ Torr. The selected area electron diffraction (SAED)

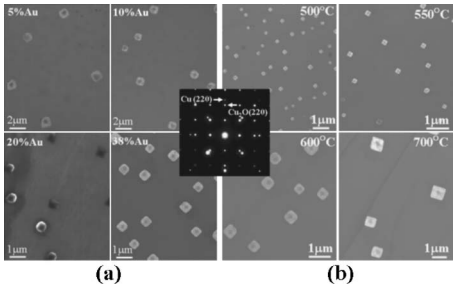

FIG. 2. (a) Oxide islands formed during oxidation of $Cu_{1-x}Au_x$ alloys at 600 °C and $pO_2=5\times10^{-4}$ Torr. (b) Oxide islands formed during oxidation Cu–38 at. % Au at $pO_2=5\times10^{-4}$ Torr, but different temperatures. The inset shows the epitaxial relationship between the Cu_2O islands and the Cu–Au substrate.

patterns reveal that the Cu_2O islands are epitaxial with the underlying substrate, i.e., $(100)Cu_2O\|(100)Cu-Au$ and $[001]Cu_2O\|[001]Cu-Au$.

We measured the saturation number density of the oxide nuclei as a function of oxidation temperature from 500 to 700 °C in $pO_2=5\times10^{-4}$ Torr. Figure 3 gives the measured saturation number density at different oxidation temperatures. The measurements indicate that the saturation density depends on the oxidation temperature; i.e., oxidation at a higher temperature results in a smaller number density of islands. On the other hand, the number density also depends on the Au mole fraction in the alloys; i.e., oxidation of alloys with higher Au mole fractions results in a larger saturation density of nuclei.

The activation energy for the nucleation of oxide islands can be deduced from the saturation island density at different oxidation temperatures. The observation that the number density of oxide nuclei saturates suggests that the nucleation process is limited by oxygen surface diffusion;[6] i.e., an active zone of oxygen capture exists around each island, and the radius of this capture zone is proportional to the oxygen surface diffusion rate. The probability of a nucleation event is proportional to the fraction of available surface area outside these zones of oxygen capture. The saturation island

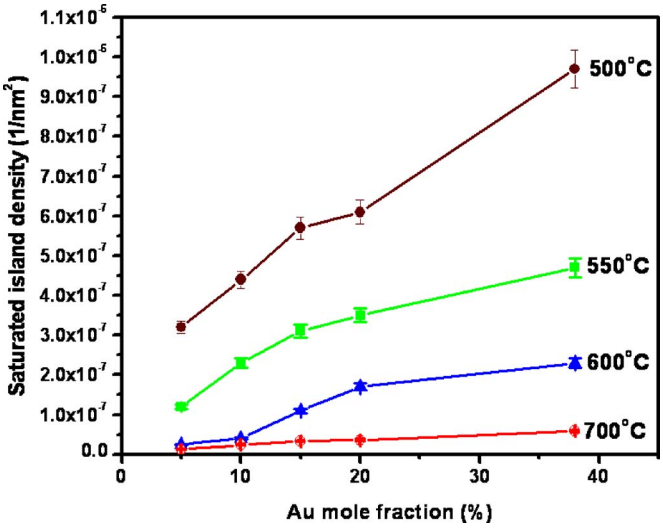

FIG. 3. (Color online) Saturation number density of oxide nuclei as a function of Au mole fractions.

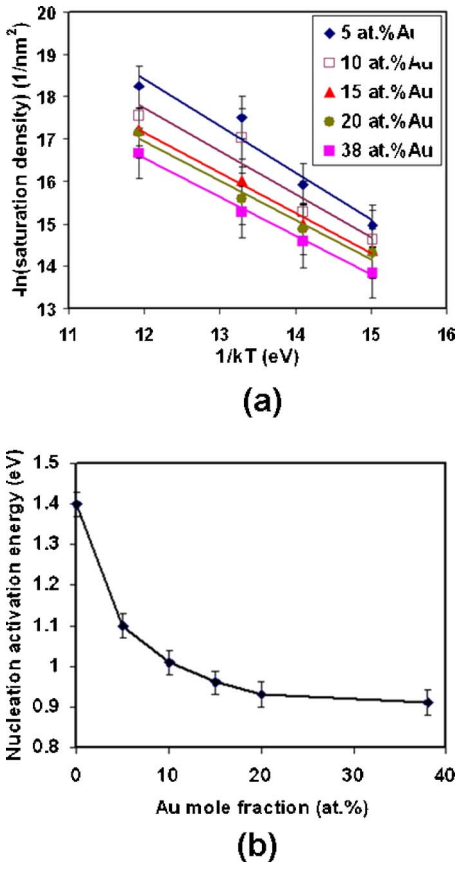

FIG. 4. (Color online) (a) Arrhenius dependence of saturation island density on oxidation temperature, the absolute value of the slope corresponds to the activation energy (E_N) for nucleation of oxide islands; (b) nucleation activation energy determined from the oxidation of the Cu–Au alloys with different Au mole fractions.

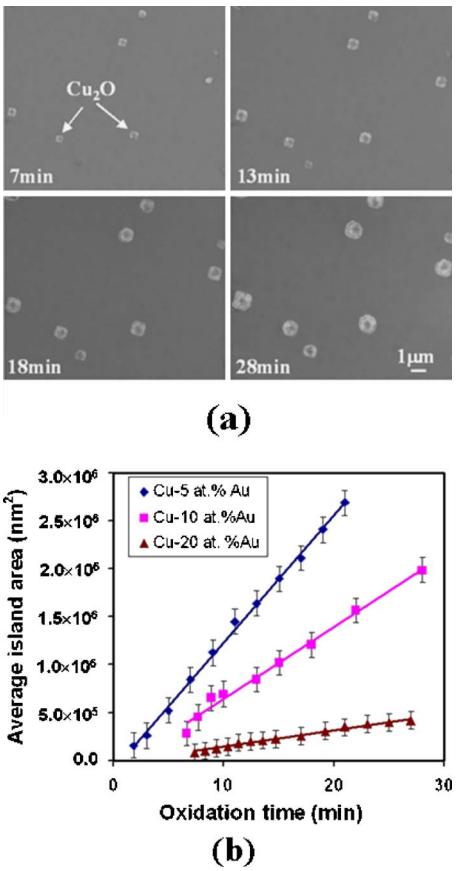

FIG. 5. (Color online) (a) *In situ* bright field TEM images showing the growth of Cu_2O islands during oxidation of (100)Cu–10% Au at 600 °C in $pO_2=5\times10^{-4}$ Torr. Note that there is a saturation of the island nuclei. (b) The average island area vs oxidation time during oxidation of the Cu–Au alloys; a linear growth behavior is noted for the different alloys. The value of the slope corresponds to the rate constant for the oxide growth.

density is reached when the zones of oxygen capture of neighboring islands impinge on each other. Due to the larger surface mobility of oxygen at higher temperatures, the radius of oxygen capture zone increases with temperature and the attachment of oxygen to existing islands is more favorable than nucleation of new nuclei. Therefore, the dependence of the saturation island density N_S on oxidation temperature follows an Arrhenius relationship,

$$N_s \sim e^{-E_N/kT}, \tag{1}$$

where k is the Boltzmann constant, T is the temperature, and E_N is the activation energy for the nucleation of oxide islands. Figure 4(a) shows the log-log plot of the saturation number density of oxide nuclei versus inverse oxidation temperature. The absolute value of the slope in Fig. 4(a) is E_N, and Fig. 4(b) shows the E_N values determined as a function of composition, which indicates that alloys with larger Au mole fractions have smaller E_N.

B. Effect of composition on the growth of oxide islands

Figure 5(a) shows *in situ* observations of the growth of individual islands during the oxidation of (100) Cu–10 at. % Au at 600 °C in $pO_2=5\times10^{-4}$ Torr. The average individual island size (area) was observed to show a linear dependence on oxidation time, as shown in Fig. 5(b). The rate constants for oxide growth, obtained from the slope of the area versus time curves in Fig. 5(b), decrease with increasing Au content. We also measured the rate constant R for oxide growth at different oxidation temperatures ranging from 500 to 700 °C in $pO_2=5\times10^{-4}$ Torr, as shown in Fig. 4(a). It is noted that alloys with higher Au mole fraction have smaller rate constants for oxide growth for oxidation at the same temperature. On the other hand, increasing the oxidation temperature results in a larger rate constant for oxide growth.

The apparent activation energy for oxide growth can be obtained by measuring the rate constant R at different oxidation temperatures. The rate constant R follows an Arrhenius dependence on oxidation temperature,

$$R \propto e^{-E_G/T}, \tag{2}$$

where E_G is the apparent activation energy for oxide growth and T is the oxidation temperature. We determined E_G by measuring R at different oxidation temperatures ranging from 500 to 700 °C in $pO_2=5\times10^{-4}$ Torr. The determined values of R are plotted as a function of reciprocal temperature in Fig. 6(b), where the apparent activation energy E_G is equal to the slope. Figure 6(c) gives the determined E_G, and it is noted that the increase of the Au mole fraction in the alloys results in a larger E_G.

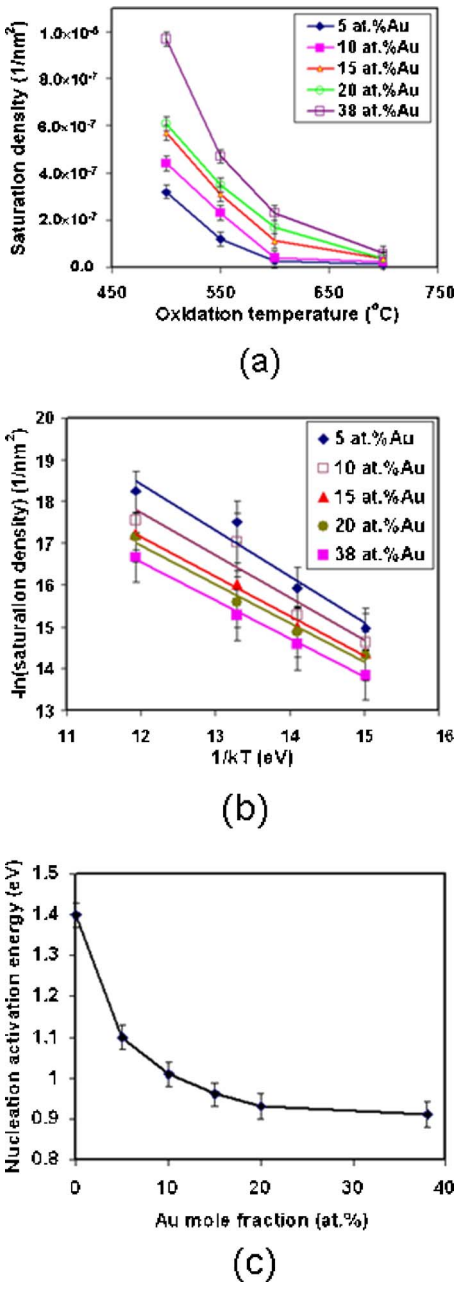

FIG. 6. (Color online) (a) Rate constants of oxide growth as a function of Au mole fraction during oxidation of the Cu–Au alloys at the different oxidation temperatures in $pO_2 = 5 \times 10^{-4}$ Torr; (b) Arrhenius dependence of the rate constants on temperature, the absolute value of the slope is the apparent activation energy (E_G) for the growth of oxide islands; (c) composition dependence of the apparent activation energy for the oxide growth during Cu–Au oxidation.

IV. DISCUSSION

A. Effect of surface segregation

The surface composition of alloys often differs from that of the bulk. This phenomenon usually obeys a few simple rules. (i) On annealing, the surface becomes enriched in the element of lower heat of sublimation or surface free energy. (ii) Ion bombardment depletes the surface of the element that exhibits a higher sputtering rate. (iii) On chemisorption, the element more strongly bound to the adsorbate will segregate to the surface.

In Cu–Au alloys, gold is characterized by lower surface free energy than copper. Thus theory predicts the segregation of Au to the surface.[13,14] Many experimental investigations of surface segregation for the Cu–Au system have demonstrated surface enrichment of Au upon vacuum annealing.[15–20] On the other hand, the more reactive element in the Cu–Au system is copper, and in the presence of any chemisorbing species such as oxygen, copper dominates at the surface. The oxidation of Cu–Au alloys in our investigation involves the situations of (i) and (iii), i.e., vacuum annealing and oxygen chemisorption. The Cu–Au alloy thin films are first annealed at high temperature (~750 °C) to remove the native oxide formed during sample preparation, and then cooled to the desired temperature for oxidation. During vacuum annealing, Au atoms segregate to the alloy surface to minimize the surface free energy. The enrichment of Au atoms turns the surface relatively inert towards oxygen chemisorption, the first step in oxide formation.[21] However, with continued exposure to oxygen, chemisorption increases due to adsorbate-induced segregation of Cu to the alloy surface.[22–24]

Clearly, compared with the oxidation behavior of pure copper, the nucleation of oxide islands during oxidation of Cu–Au alloys involves additional processes, such as surface segregation of Cu induced by O chemisorption and Au diffusion away from the surface layer. Therefore, it is reasonable to expect that a longer incubation period is needed for the nucleation of oxide islands during oxidation of Cu–Au alloys and that increasing the Au mole fraction will also result in increased incubation times for oxide nucleation. This scenario is consistent with our *in situ* TEM observations of the composition dependence of the incubation time.

B. Effect of Au on nucleation of oxide islands

In order to form oxide islands on metal surface, the system must overcome an activation barrier whose height is given by the work of formation of the critical-sized nuclei. The number of critical nuclei per unit area is

$$N_{r^*} = N_0 \exp\left(-\frac{E_N}{kT}\right), \tag{3}$$

where r^* is the radius of the critical nucleus, N_0 is the number of nucleation sites per unit area of the substrate surface, E_N is the free energy of formation of a critical-sized nucleus, and k and T have their usual meanings. The main contributions to E_N are the volume free energy, surface/interfacial free energy, and interfacial strain energy during the formation of an oxide nucleus. By considering heterogeneous nucleation of an oxide island on an alloy surface, this activation energy can be easily obtained as

$$E_N = f(\theta)\sigma^3 \frac{1}{(\Delta G_V + \Delta G_S)^2}, \tag{4}$$

where $f(\theta)$ is a geometric factor dependent on the surface and interfacial energies, σ is the average surface energy of oxide, ΔG_V is the free-energy change that drives the oxidation reaction, and ΔG_S is the strain energy due to the lattice mismatch between the oxide and the metal substrate. ΔG_V

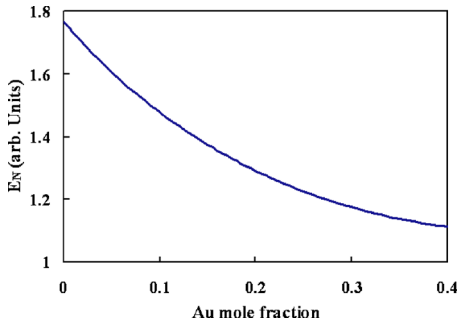

FIG. 7. (Color online) Dependence of nucleation barrier E_N on Au mole fraction during oxidation of Cu–Au alloys.

can be determined for the oxidation reaction $2Cu_{1-x}Au_x + 1/2O_2 = Cu_2O$ by assuming an ideal solution behavior of Cu–Au alloys,

$$\Delta G_V = V \times \left(\Delta G^0 - 2RT \ln(1 - x_{Au}) - \frac{RT}{2} \ln pO_2 \right), \quad (5)$$

where V is the volume of the oxide nucleus, ΔG^0 is the standard free energy change for Cu_2O formation, R is the gas constant, T is the oxidation temperature, x_{Au} is the mole fraction of Au in the $Cu_{1-x}Au_x$ alloy, and pO_2 is the oxygen partial pressure.

The strain energy ΔG_S in an oxide island due to the lattice mismatch is proportional to $(E/1-\nu)\varepsilon^2$, where E and ν are Young's modulus and the Poisson ratio of Cu_2O, respectively, and ε is the lattice mismatch between Cu_2O and the substrate. According to Vegard's law, the lattice constant of a $Cu_{1-x}Au_x$ solution is

$$a_{Cu_{1-x}Au_x} = a_{Au}x_{Au} + a_{Cu}(1 - x_{Au}), \quad (6)$$

where, at room temperature, a_{Cu}=3.61 Å, a_{Au}=4.02 Å, and a_{Cu_2O}=4.22 Å, and x_{Au} is the mole fraction of Au in the alloy. The lattice constant of a Cu–Au alloy increases with increasing Au content and the lattice mismatch ε between the oxide and the substrate is correspondingly reduced. By applying the above derivation and plotting the nucleation activation barrier E_N as a function of the Au mole fraction, we can determine the effect of Au on the nucleation thermodynamics of oxide islands, as shown in Fig. 7, which shows that increasing the Au mole fraction in the alloy leads to a decrease in the nucleation barrier, qualitatively consistent with the experimental measurements of the nucleation activation energies obtained from the Arrhenius dependence of the saturation island density on oxidation temperature [Fig. 4(b)].

C. Effect of Au on oxide growth

Au does not form a stable oxide under most conditions and does not go into solution in the oxide phase due to its stable electronic configuration. As a result, oxidation of Cu–Au alloys results in selective oxidation of Cu and in rejection of Au from the metal-oxide interface, leading to Au enrichment in the remaining alloy. This enrichment of Au around the oxide islands is confirmed by an elemental analysis. Figure 8(a) shows an oxide island formed during oxidation of Cu–10% Au at 600 °C. The dark contrast around the island is due to the accumulation of Au atoms segregated from the metal-oxide interface during the oxide growth. The contrast features in Fig. 8(a) reveal that there is a nonuniform partition of Au atoms in the alloy around the island, and alloy regions adjacent to the island edges have more Au accumulation than those adjacent to the island corners, as confirmed by energy dispersive x-ray spectroscopy (EDS) shown in Fig. 8(b). This nonuniform Au partition that develops as Cu–Au alloy oxidation proceeds is qualitatively consistent with a two dimensional analysis based on Fick's diffusion laws, and the compositional inhomogeneity leads to a distinct change in Cu_2O island morphology from an initial square shape as oxidation progresses.[25]

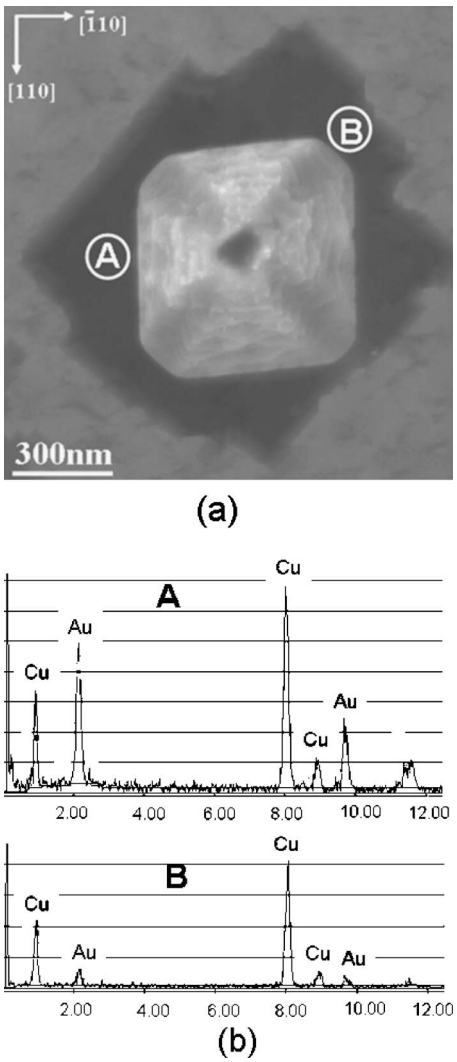

FIG. 8. Elemental analysis of one oxide island formed at 600 °C during oxidation of Cu–10% Au. Quantification of the EDS indicates that region A has a Cu/Au ratio of 0.7, and region B has a ratio of 4.8, revealing a nonuniform enrichment of Au in the alloy regions adjacent to island corners and edges.

Since the oxide growth is accompanied by the rejection of Au atoms from the metal-oxide interface, increasing the Au mole fraction in the alloys leads to the rejection of more Au atoms from the oxide phase for the formation of the same amount of Cu_2O by comparison with the alloys with less Au. Also, since Au does not show a strong affinity with oxygen,

increasing the Au mole fraction leads to a reduced surface sticking coefficient of oxygen, which in turn leads to a reduced oxygen surface diffusion flux to the metal-oxide interface for the oxide growth. All of these factors contribute to the observed decreased growth rate and the increased apparent activation energy for the oxide growth in the alloy with more Au.

D. Effect of Au on the passivation behavior of Cu–Au alloys

Previous studies of copper alloys, which sought to improve oxidation resistance, found that Cu–Be, Cu–Mg, Cu–Cr, Cu–Si, Cu–Ti, Cu–Cr, Cu–Pd, and Cu–Al systems are more resistant to oxidation than pure Cu, whereas the Cu–Au system does not show a self-limiting behavior.[26–28] Studies of the bulk oxidation behavior of pure copper have revealed that oxidation effectively stops after a certain time interval, whereas studies of bulk Cu–Au alloys have found that oxidation (of Cu) continues until complete decomposition of the alloys occurs.[29] For most of the systems listed above Cu is the more noble component of the alloy. However, Cu–Pd is similar to Cu–Au in that Cu is the more reactive component in the alloy; therefore, passivation behavior is not determined simply by whether the second component in the alloy is more or less noble than Cu. While previous studies have demonstrated that the oxide formed on Cu–Au alloy surfaces does not provide protection from further oxidation, they have not identified a mechanism to explain the decreased passivation property of the oxide layer on Cu–Au alloys. Our present results provide important insight into this issue.

The nonprotective properties of the oxide layer on Cu–Au surfaces can be understood from the microstructure of the oxide film, which is directly related to the early-stage oxidation behavior. Our present investigation indicates that gold enhances the nucleation of oxide islands and suppresses the oxide growth rate. As oxidation continues, particularly at large oxygen partial pressure, islands may impinge while still quite small in their lateral dimension (and thickness). A large number of interfaces are formed in the oxide film due to the accumulation of rejected Au atoms around the oxide islands, which prevents the perfect coalescence of the islands. Furthermore, we have also observed that the compositional inhomogeneity that develops as Cu–Au alloy oxidation proceeds may lead to a discontinuous morphology of the oxide layer through a dendritic transition from initially compact Cu_2O islands.[25] The outward diffusion of copper atoms along these interfaces, other defects, and discontinuities in the oxide layer is likely much faster than through a perfectly coalesced oxide film; hence protection from further oxidation does not occur for Cu–Au alloys.

V. CONCLUSIONS

The kinetics of early-stage oxidation of Cu–Au alloys was investigated using *in situ* UHV-TEM. Our observations indicate that the incubation time associated with the formation of visible oxide nuclei on the alloy surfaces increases with Au mole fraction in the alloys. Measurements of nucleation and growth rates of oxide islands have revealed that increasing the Au mole fraction in the alloys results in an increase in the number density of oxide nuclei, but a decrease in the island growth rate. We expect that the present results may also be relevant to the behavior of other alloys comprised of both reactive and noble elements.

ACKNOWLEDGMENTS

Argonne National Laboratory's work was supported by the U.S. Department of Energy, Office of Science, Office of Basic Energy Sciences under Contract No. W-31-109-Eng-38. The *in situ* TEM experiments were performed at the Materials Research Laboratory, University of Illinois at Urbana-Champaign, which is supported by the U.S. Department of Energy (DEFG02-96-ER45439). The authors thank R. Twesten and K. Colravy for their help.

[1] C. Wagner, Z. Phys. Chem. Abt. B **21**, 25 (1933).
[2] W. W. Smeltzer, R. R. Haering, and J. S. Kirkaldy, Acta Metall. **9**, 880 (1961).
[3] J. Stringer, in *Point Defects and Transport in Oxides*, edited by M. S. Seltzer and R. J. Jaffee (Plenum, New York, 1974), pp. 495–517.
[4] J. Atkinson, Rev. Mod. Phys. **57**, 437 (1985).
[5] J. C. Yang, M. Yeadon, B. Kolasa, and J. M. Gibson, Appl. Phys. Lett. **70**, 3522 (1997).
[6] J. C. Yang, M. Yeadon, B. Kolasa, and J. M. Gibson, Scr. Mater. **38**, 1237 (1998).
[7] J. C. Yang, B. Kolasa, J. M. Gibson, and M. Yeadon, Appl. Phys. Lett. **73**, 2841 (1998).
[8] G. W. Zhou and J. C. Yang, Phys. Rev. Lett. **89**, 106101 (2002); Appl. Surf. Sci. **210**, 165 (2003); Phys. Rev. Lett. **93**, 226101 (2004); Surf. Sci. **531**, 359 (2003); Appl. Surf. Sci. **222**, 357 (2004); Surf. Sci. **559**, 100 (2004).
[9] N. Cabrera and N. F. Mott, Rep. Prog. Phys. **12**, 163 (1948).
[10] M. L. McDonald, J. M. Gibson, and F. C. Unterwald, Rev. Sci. Instrum. **60**, 700 (1989).
[11] G. W. Zhou and J. C. Yang, Phys. Rev. Lett. **93**, 226101 (2004).
[12] S. M. Francis, F. M. Leibsle, S. Haq, N. Xiang, and M. Bowker, Surf. Sci. **315**, 284 (1994).
[13] M. Polak and L. Rubinovich, Surf. Sci. Rep. **38**, 129 (2000).
[14] U. Bard, Rep. Prog. Phys. **57**, 939 (1994).
[15] H. Reichert, P. J. Eng, H. Dosch, and I. K. Robinson, Phys. Rev. Lett. **74**, 2006 (1995).
[16] N. Igata, Nanotechnology **7**, 21 (1996).
[17] T. M. Buck and G. H. Wheatley, Phys. Rev. Lett. **51**, 43 (1983).
[18] S. Y. Li and R. S. Li, Surf. Interface Anal. **27**, 957 (1999).
[19] J. M. McDavid and S. C. Fain, Surf. Sci. **52**, 161 (1975).
[20] I. K. Robinson and P. J. Eng, Phys. Rev. B **52**, 9955 (1995).
[21] J. A. Eastman, P. H. Fuss, L. E. Rehn, P. E. Baldo, G.-W. Zhou, D. D. Fong, and L. J. Thompson, Appl. Phys. Lett. **87**, 051914 (2005).
[22] G. Graham, Surf. Sci. **137**, L79 (1984).
[23] S. Nakanishi, K. Kawamoto, N. Fukuoka, and K. Umezawa, Surf. Sci. **261**, 342 (1992).
[24] H. Niehus and C. Achete, Surf. Sci. **289**, 19 (1993).
[25] G.-W. Zhou, L. Wang, R. C. Birtcher, P. E. Baldo, J. E. Pearson, J. C. Yang, and J. A. Eastman, Phys. Rev. Lett. **96**, 226108 (2006).
[26] J. Li, J. W. Mayer, and E. G. Colgan, J. Appl. Phys. **70**, 2820 (1991).
[27] K. W. Frohlich, Z. Metallkd. **28**, 368 (1936).
[28] C. Wagner, J. Electrochem. Soc. **99**, 369 (1952).
[29] J. Janczak and R. Kubiak, J. Alloys Compd. **182**, 289 (1992).